Polymer 49 (2008) 2211–2216

Contents lists available at ScienceDirect

Polymer

journal homepage: www.elsevier.com/locate/polymer

One-step synthesis of functional Co nanoparticles for surface-initiated polymerization

Celin Gürler [a], Mathias Feyen [a,1], Silke Behrens [b], Nina Matoussevitch [b,2], Annette M. Schmidt [a,*]

[a] Institut für Organische und Makromolekulare Chemie, Heinrich-Heine-Universität, Universitätsstr. 1, D-40225 Düsseldorf, Germany
[b] Institut für Technische Chemie (ITC-CPV), Forschungszentrum Karlsruhe GmbH, Postfach 3640, 76021 Karlsruhe, Germany

ARTICLE INFO

Article history:
Received 18 January 2008
Received in revised form 5 March 2008
Accepted 6 March 2008
Available online 18 March 2008

Keywords:
Surface-initiated polymerization
Field-induced rotation
Core–shell particles

ABSTRACT

Much effort is conducted to construct artificial objects that are capable of converting chemical or electromagnetic energy into a specific, predetermined motion on the nanoscale. We present results on the synthesis of core–shell nanoparticles capable to be set in rotation by the application of electromagnetic fields. The nanorotors implied in the study are based on the cobalt nanospheres decorated with a stabilizing brush shell composed of poly(ε-caprolactone) that is attached by surface-initiated polymerization. The functional cores used as macroinitiators can be fabricated alternatively by a two-step or a one-step process.

1. Introduction

Organic–inorganic hybrid materials incorporating magnetic nanoparticles are of growing interest in actual materials research due to the unique properties including magnetic manipulation, detection, and field-induced local heating processes. There is need for synthetic pathways that allow the preparation of well-defined particles with narrow size distribution, good stability and a defined interface to the liquid or solid particle environment. Such systems are of high interest concerning the magnetic separation of biological species [1] or catalysts and for the purification of wastewater [2,3].

In alternating fields in the kHz to GHz range, magnetic nanoparticles undergo a reversal of their moment driven by the rotation of the field vector resulting in a local evolution of thermal energy. Concerning spherical Co particles with a diameter of 8 nm and more, the magnetic anisotropy barrier is high enough to consider the particles' moment to be blocked inside the crystal lattice of the particle [4]. As a consequence, such systems are forced to a fast, Brownian-like rotation of the whole particle in alternating fields. As such, the characteristic time scale of such process depends on the hydrodynamic radius of the particles and the inner viscosity of the system [5]. Thus, the time-dependent field is partially transformed into kinetic energy of the particles.

Cobalt nanoparticles in the nanometer size range are commonly prepared by the reduction of cobalt salts or by the thermal composition of $Co_2(CO)_8$, in the presence of either low molecular or polymeric surfactants, firstly described as early as 1966 [7,8]. In particular, micelle-forming copolymers have been applied to the synthesis, and it has been shown in several systematic investigations that the choice of block polarity, molecular weight and concentration is suitable to optimize particle size and size distribution for the respective needs [9–13]. Similar findings have been reported for polymer coated iron particles starting from $Fe(CO)_5$ [14,15].

In view of the above-mentioned applications, however, there is need for polymer shells that perform more sophisticated functions, and much effort has been conducted for the development of well-defined polymer shells with predetermined architecture, thickness and chemical functionality. A versatile method for the preparation of polymer shells with a brush architecture, that combines high grafting density, adjustable thickness and effective steric stabilization, is surface-initiated polymerization, realized by the surface attachment of initiator groups and subsequent chain growth according to an appropriate mechanism [16]. Due to its controlled character and the high monomer versability resulting from the good tolerance towards many functional groups, atom transfer radical polymerization (ATRP) is the most widely applied method for the creation of polymer brushes on particulate surfaces [17–20]. The use of ring-opening polymerization (ROP) has also been shown to result in well-defined brush layers [21–24] and is suitable for the synthesis of polyester brush coatings on ferrite particles [25,26]. In

* Corresponding author. Tel.: +49 (0)211 81 14820; fax: +49 (0)211 81 15840.
E-mail address: schmidt.annette@uni-duesseldorf.de (A.M. Schmidt).
[1] Present address: Max-Planck-Institut für Kohleforschung, Kaiser-Wilhelm-Platz 1, D-45470 Mühlheim an der Ruhr, Germany.
[2] Present address: Qiagen GmbH, Qiagenstraße 1, D-40724 Hilden, Germany.

0032-3861/$ – see front matter © 2008 Elsevier Ltd. All rights reserved.
doi:10.1016/j.polymer.2008.03.012

these studies, the initiator sites are introduced to the particle surface in an additional step after core precipitation.

In this work, we show that the hybrid cobalt/polycaprolactone brush particles can be obtained and effectively stabilized in toluene dispersion by two different pathways. Next to the surface functionalization of particles subsequent to precipitation, we show that hydroxy-functional cobalt cores can be obtained in a single step by thermal decomposition of $(Co)_2(CO)_8$ in the presence of ricinolic acid as a functional surfactant. The role of ricinolic acid is multifold: (1) it serves as micelle-forming pre-stabilizing amphiphile for the decomposition, (2) it allows a permanent attachment on the particle surface oxide layer by means of the carboxyl function, (3) provides an effective steric stabilization due to the aliphatic chain, and (4) enables subsequent surface-initiated ring-opening polymerization of lactones by using the hydroxyl group.

This way, polymer brushes are created on the particle surface with a high degree of synthetic flexibility concerning composition and thickness of the shell. We show that hydrodynamic properties of the dispersions that are ruled by the polymer shell thickness influence the dynamic magnetic properties of the hybrid materials. Therefore, we investigated magnetic heating characteristics in AC magnetic fields on a set of core–shell materials based on the same batch of cobalt core and with different shell thicknesses.

2. Experimental part

2.1. Materials and instrumentation

Dicobaltoctacarbonyl (95%) stabilized in 5% hexane (Sigma), ricinolic acid (85%; TCI), 1,2-dichlorobenzene (99%; Aldrich), trioctylphosphineoxide (99%; Acros Organics) and tin(II)-bis(2-ethylhexanoate) were used as-received. Ricinolic acid and dicobaltoctacarbonyl were stored at −20 °C. Acetone was dried with phosphorous pentoxide (98%; Acros Organics) and distilled. Dry acetone was stored under Argon with molecular sieves 3 Å. ε-Caprolactone (98%; Merck) was dried with calcium hydride (92%; Riedel-de-Haën) and distilled *in vacuo*. Xylene (Riedel-de-Haën) was used as-received.

Attenuated total reflection FTIR (ATR-FTIR) is conducted on Nicolet FT-IR 5SXB equipped with a diamond. Nuclear magnetic resonance spectra were recorded on a Bruker DRX500 at ambient temperature with TMS as internal standard. Gel permeation chromatography (GPC) is conducted in tetrahydrofurane with a system consisting of a SFD sample collector, a pump (Waters 510, 1 ml min^{-1}) using polystyrene coulombs of 100 Å, 1000 Å and 10 000 Å and a differential refractometer detector (Waters), relative to polystyrene calibration. Elemental analysis (EA) is performed on a Perkin–Elmer analyzer 2400. Dynamic Light Scattering (DLS) is measured on a Malvern Instruments HPP5002 at $\lambda = 633$ nm at 25 °C. The presented results on the hydrodynamic diameter d_v are volume-averaged. TEM experiments are performed on samples prepared by drop-casting on a carbon-coated 400 mesh copper grid by using a Philips Tecnai F20 equipped with a field emission gun at 200 kV.

2.2. Synthesis procedures

All synthetic procedures are performed under argon atmosphere.

2.2.1. Synthesis of cobalt nanoparticles

The cobalt particles are synthesized by thermal decomposition of dicobaltoctacarbonyl $Co_2(CO)_8$ by two different methods. They are obtained either (PF route) by a method according to Bönnemann et al. [27] and received as a powder. In a typical procedure, 0.5 g $Co_2(CO)_8$ (1.5 mmol) is added to 0.25 ml $Al(C_8H_{17})_3$ in 8.7 ml toluene and heated to reflux for 22 h under stirring. After cooling the reaction mixture to room temperature, the particles are passivated by synthetic air, which was carefully introduced through a small capillary. The resulting black precipitate is washed several times with toluene. In the second step, the particles are stabilized by ultrasonic radiation in the presence of ricinolic acid, followed by repeated washing cycles in ethanol in order to remove excess surfactant, and redispersed in toluene.

Alternatively, the stabilized and hydroxy-functional particles can be obtained in one step after a procedure of Puntes et al. [28] by replacing oleic acid with ricinolic acid (DF route). In this procedure, 0.5 g dicobaltoctacarbonyl ($Co_2(CO)_8$) is dissolved in 3 ml 1,2-dichlorobenzene in a 25 ml Schlenk-flask. Trioctylphosphine oxide (0.1 g, 0.26 mmol) and 0.2 ml (0.63 mmol) ricinolic acid are dissolved in 12 ml 1,2-dichlorobenzene and heated to reflux under stirring. The solution of dicobaltoctacarbonyl is rapidly injected. After 30 min of heating, the reaction mixture is cooled down to ambient temperature. The obtained black ferrofluid has a cobalt mass content of about 172 mg and a particle concentration of 1.1 mass%.

The ricinolic acid-functional particles are precipitated in a threefold volume of acetone. Afterwards the product is washed with acetone several times, and the obtained particles are redispersion in toluene.

2.2.2. Surface-initiated ring-opening polymerization of ε-caprolactone

Ricinolic acid (0.65 ml) functional Co particles dispersed in 1.35 ml toluene are placed in a two-neck flask, and the required amount of 0.2 ml (1.8 mmol) ε-caprolactone and 0.73 mg (1.8 μmol) tin(II)-bis(2-ethylhexanoate) as the catalyst is added. Afterwards, the mixture is heated to 130 °C and polymerized for 5 h. After cooling to room temperature, the particles are purified by precipitation in hexane and redispersed in toluene, followed by dropwise addition of ethanol at 0 °C and magnetic separation of the precipitated particles in order to remove free polymer chains.

2.2.3. Acidolysis of Co cores

In order to characterize the polymer arms, 0.3 ml toluene-dispersed core–shell particles are treated with the same volume of 1 M hydrochloric acid that is added dropwise to the heavily stirred dispersion. The mixture is stirred until the black colour is disappeared and a bluish aqueous phase can be separated from the organic, polymer-containing phase. The aqueous phase is washed several times with toluene, and the organic fractions with 1 M hydrochloric acid, brine, and water. The polymer is obtained by drying the organic phase *in vacuo* and analyzed with ^1H NMR, ATR-FTIR and GPC.

3. Results

We report the synthesis and properties of cobalt nanoparticles with a poly(ε-caprolactone) (PCL) brush shell of variable thickness by two different pathways, and investigate the influence of preparation procedure and particle radius on the dispersion properties.

3.1. Particle synthesis

By the precipitation–functionalization method (PF), a three-step procedure is followed by first thermolysis of $Co_2(CO)_8$ in the presence of trioctylaluminum and subsequent smooth oxidation [27]. The aluminum alkyls on the one hand act as an activator for the decomposition of the cobalt precursor, and on the other improves the surface passivating oxidation of the particles, preventing a further oxidation of the cobalt core in the presence of oxygen. The toluene-suspended Co nanoparticles with a diameter of 10 nm (TEM)

were surface-functionalized with ricinolic acid by chemisorption of the carboxylic acid group in order to introduce hydroxyl groups that serve as an initiator for the ring-opening polymerization of ε-caprolactone.

Alternatively, an additional functionalization step can be avoided by direct functionalization (DF method) during the thermolysis of $Co_2(CO)_8$ in the presence of ricinolic acid by adapting a procedure of Puntes et al. [28]. In contrast to the particles used in PF route, these nanoparticles are not surface passivated, and as a consequence they have to be handled under inert atmosphere to prevent their oxidation.

Both pathways result in stable dispersions of functional Co particles in toluene, with Co contents of 0.3 mass% and 0.7 mass%, respectively (see Table 1). The presence of ricinolic acid on the particle surface can be verified qualitatively by ATR-FTIR, and quantified by elemental analysis.

Comparison of the ATR-FTIR spectra (Fig. 1) shows significant similarities between the two species of functional Co particles and ricinolic acid indicating successful immobilization on the particle surface in both cases. Differences in the relative intensities of the peaks are attributed to possible differences in the actual binding mode on the surface and to the restricted mobility of the alkyl chains in the confinement of the surface.

From elemental analysis, the organic mass content and from this the surface functionality on ricinolic acid for both types of Co particles can be extracted. We obtain a value of 0.49 mmol g^{-1} for particles obtained after the PF method, and a slightly higher value of 0.60 mmol g^{-1} for DF particles, showing a good functionalization degree suitable for the following step of polymer shell synthesis.

3.2. Surface-initiated polymerization

The ricinolic acid-functional Co particles carry a large number of hydroxyl groups and thus they are capable to serve as multifunctional macroinitiators for the surface-initiated ring-opening polymerization of ε-caprolactone. This synthetic pathway is suitable for the preparation of polymer brush shells of high grafting density and adjustable thickness [25]. By choice of the particle-to-monomer ratio, the arm length of the polymer brush shell can be tailored and thus the hydrodynamic radius is influenced.

This way, cobalt nanoparticles obtained from the PF and DF methods have been decorated with polymeric brush shells of variable thickness (Fig. 2) and were analyzed with respect to their

Table 1
Composition and properties of Co@RA and Co@PCL core–shell particles

Run	$\mu_{Co,dry}$ (mass%)	d_v (nm)	M_n (g mol^{-1})	M_s (kA m^{-1})	$\mu_{Co,disp}$ (mass%)	d_c (nm)
Method PF						
$Co@RA_{PF}$[a]	83.00[a]	15.9	n.d.	0.47	0.31	9.8
$Co@PCL13_{PF}$	39.7	22.1	1300	n.d.	n.d.	n.d.
$Co@PCL17_{PF}$	28.1	25.2	1700	1.20	0.90	9.9
$Co@PCL23_{PF}$	23.0	26.3	2300	2.06	1.58	10.1
$Co@PCL27_{PF}$	18.5	30.9	2700	2.88	1.97	10.0
$Co@PCL32_{PF}$	13.7	38.5	3200	3.71	2.83	9.9
Method DF						
$Co@RA_{DF}$[a]	87.3	10.3	n.d.	1.11	0.71	11.4
$Co@PCL14_{DF}$	39.6	20.7	1350	n.d.	n.d.	n.d.
$Co@PCL16_{DF}$	37.6	21.1	1600	n.d.	n.d.	n.d.
$Co@PCL24_{DF}$	23.8	27.2	2400	n.d.	n.d.	n.d.
$Co@PCL48_{DF}$	9.4	54.6	4800	n.d.	n.d.	n.d.

$\mu_{Co,dry}$: cobalt mass content of dry particles, from TGA; d_v: volume-average hydrodynamic diameter, from DLS; M_n: number-average molar mass of polymer arms, from GPC; M_s: saturation magnetization; $\mu_{Co,disp}$: cobalt mass content of dispersions, from VSM; d_c: core diameter from VSM.
Nomenclature: Co@RA, ricinolic acid-functionalized cobalt nanoparticles; Co@PCLxy, cobalt nanoparticles with a poly(ε-caprolactone) brush shell; xy = M_n: 100; n.d., not determined.
[a] By elemental analysis (C content).

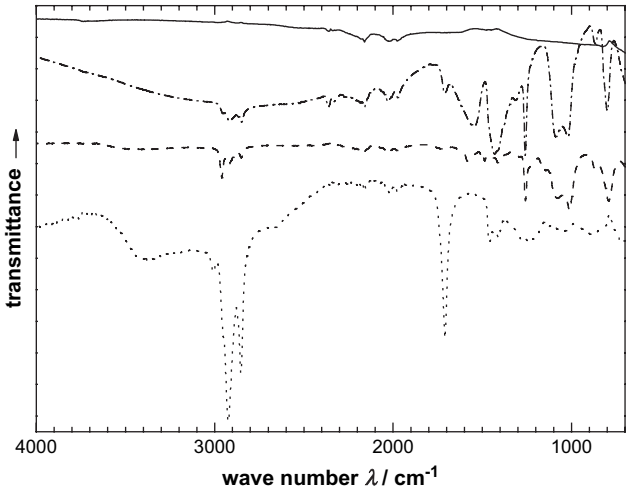

Fig. 1. ATR-FTIR spectra of bare PF particles (compact), ricinolic acid (RA, dotted) and RA-functionalized particles ($Co@RA_{PF}$: dash-dotted, $Co@RA_{DF}$: dashed).

composition, dispersion properties and their quasi-static and dynamic magnetic properties.

Therefore, repeatedly washed samples have been subjected to ATR-FT infrared spectroscopy, thermogravimetric analysis (TGA) and elemental analysis to verify the attachment of the shell and to quantify the mass ratio of polymer and inorganic core material. In order to get information on the nature of the polymeric shell, a sample of each material is subjected to acidolysis of the core with hydrochloric acid and isolation of the polymeric material. Biphasic conditions were chosen in order to prevent the polyester chains from degrading during the acidolysis, and linear PCL was treated similarly to ensure no significant change of the molecular weight or the distribution occurred [25]. The isolated polymeric fraction is subsequently characterized by proton resonance spectroscopy (^{1}H NMR) and gel permeation chromatography (GPC). ATR-FTIR confirms the presence of PCL in all samples.

A linear increase in the number-average molar mass M_n of the isolated polymer arms with growing polymer-to-cobalt ratio is detected by GPC (Fig. 3), being in accordance with the assumption of a constant grafting density of chains on the particle surface. In all cases, the polydispersity index concerning the polymer chain length is close to 2, as commonly observed in Sn-catalyzed ring-opening polymerization processes of ε-caprolactone as a consequence of the applied ROP mechanism that is characterized by interchain transesterification. It is important to stress that this

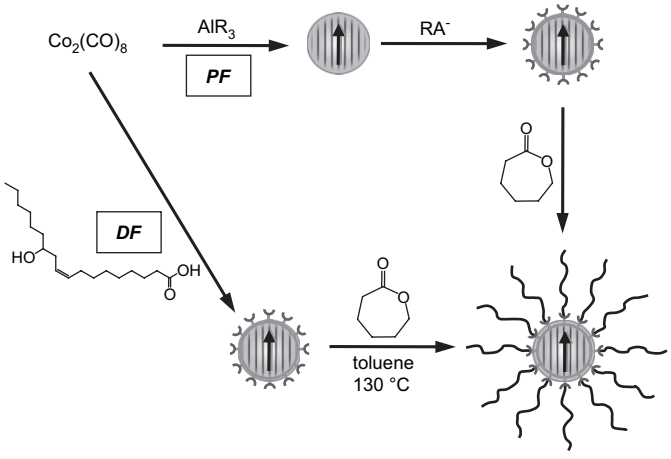

Fig. 2. Two different pathways for the synthesis of Co@PCL brush particles. PF: precipitation–functionalization, DF: direct functionalization.

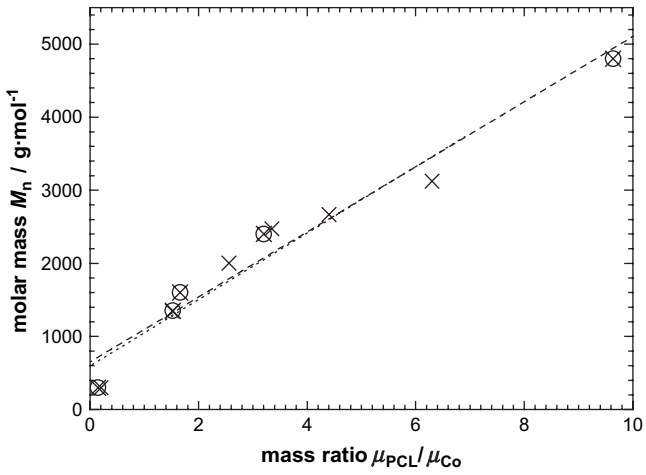

Fig. 3. Linear dependence of molar mass M_n (GPC) on the polymer-to-cobalt mass ratio.

transesterification process does not affect the surface attachment of the participating chains if both chains are attached by their carboxylic end [25].

The grafting density f_s can be calculated from the slope of the graph of M_n vs. polymer-to-cobalt ratio μ_{PCL}/μ_{Co} by using:

$$f_s = \frac{\mu_{PCL}}{\mu_{Co}} \frac{1}{M_n} \quad (1)$$

resulting in a value 0.22 ± 0.02 mmol g^{-1} for the PF samples and 0.22 ± 0.03 mmol g^{-1} for DF samples, with respect to the cobalt cores. The values are very similar for the two types of Co initiating cores, but considerably lower than the calculated surface density of ricinolic acid obtained by elemental analysis (see above), indicating that not all the surface bound moieties take part in the initiation process. Taking into account an average particle mass of ca. 4.7×10^{-18} g (with $d_c = 10$ nm, $\rho_{Co} = 8.9$ g cm^{-3}) and an average surface area of ca. 300 nm^2, this corresponds to 600 chains per particle or 2 chains per nm^2. Results on the composition of the hybrid core–shell particles are summarized in Table 1.

3.2.1. Atomic force microscopy and transmission electron microscopy

Visualization of the prepared materials and additional and complementary information on the size of core and shell of the hybrid particles are achieved by means of atomic force microscopy (AFM) and transmission electron microscopy (TEM). As shown in Fig. 4a, spherical objects are detected in AFM experiments with an average diameter of 30.3 ± 4.5 nm for Co@PCL27, which is in good agreement with DLS results (see Table 1). The shell is supposed to be stretched out in AFM experiments due to solvation with xylene (a good solvent for PCL). In contrast to this, the polymeric shell is collapsed in samples prepared in the dry state for TEM experiments (see Fig. 4b and c). The average core diameter obtained by TEM is 9.8 ± 1.4 nm (inner) and 12.9 ± 2.1 nm (outer diameter). The brighter regions are interpreted as cobalt oxide layer of the cores prepared according to the PF route, while the polymer is not visible in the TEM images. It is observed that the particles form arrays with a regular structure with enhanced interparticle distance compared to the particles without polycaprolactone, Co@RA. In Fig. 4b we extract average core center distances of 20.1 ± 2.5 nm for Co@PCL27$_{PF}$ particles, indicating a shell contribution of 7.2 nm to the total diameter in the dry state.

3.2.2. Dynamic light scattering

In order to get information on the dispersion behavior of core–shell particles with different polymer arm lengths, the hybrids were dispersed in toluene and analyzed by dynamic light scattering (DLS). The results are shown in Fig. 5 and indicate that the hydrodynamic particle diameter increases from 15.9 nm to 38.5 nm for hybrid particles obtained after the PF method, and from 10.3 nm to 54.6 nm for the DF method.

In both cases, a steady increase of the hydrodynamic diameter as obtained from DLS experiments with the molecular weight of the polymer arms is observed, in accordance with the expectation from theoretical considerations for polymer brushes grown on spherical nanoobjects. Here, the well-established blob model of Alexander [30] and de Gennes [31], resulting in a layer thickness of l_{blob}, is adapted to curved surfaces owing to the fact that the free volume of polymer chains increases with higher curvature and with distance to the surface.

Thus, the layer thickness l_{bp} of a polymer brush on a curved surface with radius r_c can be written as [32]:

$$l_{bp} = \left(\left(1 + \frac{5}{3} \frac{l_{blob}}{r_c} \right)^{\frac{3}{5}} - 1 \right) r_c \quad (2)$$

Fig. 5b shows a good accordance of the obtained results with the theoretical expectations.

3.2.3. Quasi-static magnetic properties

In vibrating sample magnetometry (VSM) experiments, the magnetization of a sample is recorded against the applied magnetic field strength in order to gain information on the response of the sample to a quasi-static and homogeneous field. The equilibrium properties of the magnetic dispersions give information on the core properties and concentration and should not be influenced by the presence of a polymeric shell, provided that the particles

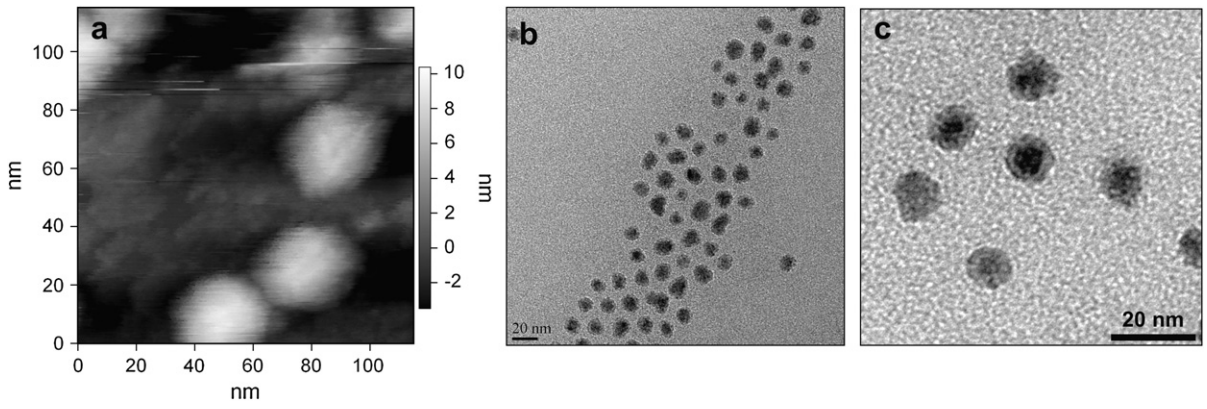

Fig. 4. AFM (a) and TEM (b and c) analyses of Co@PCL27 core–shell particles.

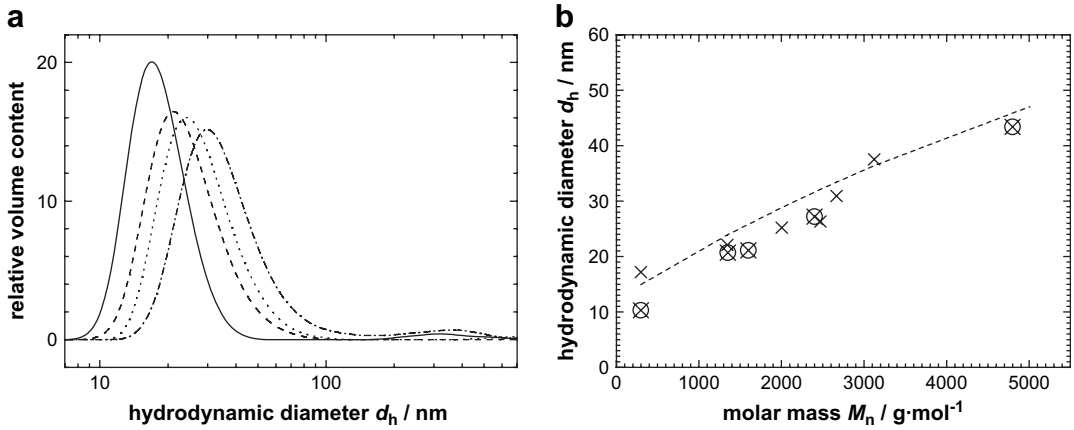

Fig. 5. Dispersion properties as determined by DLS. (a) Hydrodynamic diameter distribution of hybrid core–shell particles, compact: Co@RA$_{PF}$, dashed: Co@PCL23$_{PF}$, dotted: Co@PCL27$_{PF}$, dash-dotted: Co@PCL32$_{PF}$; (b) relationship between average hydrodynamic diameter d_h and molar mass of the polymer arms. Cross: PF particles, circled cross: DF particles, dotted: calculated (see text).

are well dispersed and able to rotate freely (Fig. 6). Information is gained on the saturation magnetization of the sample by extrapolation of M to H → ∞, and on the volume-average magnetic moment m_v of the involved particles from the initial slope of the graph.

No hysteresis is observed for all investigated samples, indicating the superparamagnetic character of the involved particles.

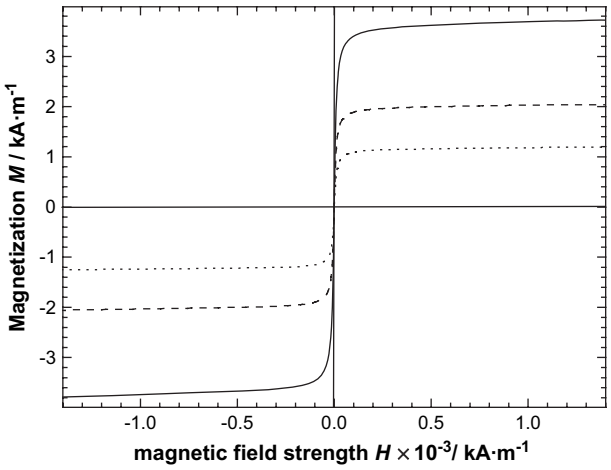

Fig. 6. Quasi-static magnetization diagram of Co@PCL17 (dotted), Co@PCL23 (dashed), and Co@PCL32 (compact) in toluene.

Magnetic fluids with a saturation magnetization of up to 3.7 kA m^{-1} were obtained. Based on the single crystal ε-Co cores ($M_0 = 1.46 \times 10^6$ A m^{-1}) [29], the cobalt content of the dispersions, $\mu_{Co,disp}$, is calculated to be up to 2.8 mass%, increasing with shell thickness. The increase of cobalt content with increasing shell thickness may be attributed to a more effective stabilization of the highly interacting magnetic particles by steric repulsion of the brushes. The initial susceptibility, that allows the calculation of the average involved magnetic moments, is extracted from the initial slope of the graph, and values for the particles' magnetic moments in the range of $7.3–7.9 \times 10^{-19}$ A m^{-1} are found, giving volume-average diameters d_c of the respective cobalt cores in all samples that are in good agreement with observations from TEM and with the unfunctionalized cores (Table 1).

3.2.4. Magnetic heating capacities of particle dispersions

The field-induced particle rotation gives an impact on the magnetic heating behavior of particles when exposed to an alternating field in the radio frequency range due to the internal friction of the rotating particles. This is shown by exposure of the samples to an AC field with fixed frequency at 300 kHz, thus well above the characteristic frequency for Brownian rotation of the particles, being below 20 kHz [6]. It is assumed that the particle radius impacts on the rotation frequency, and thus the particles are forced to a rotation limited by their hydrodynamic radius.

In order to investigate this, the temperature of the fluids is recorded against time, giving information on the specific heating

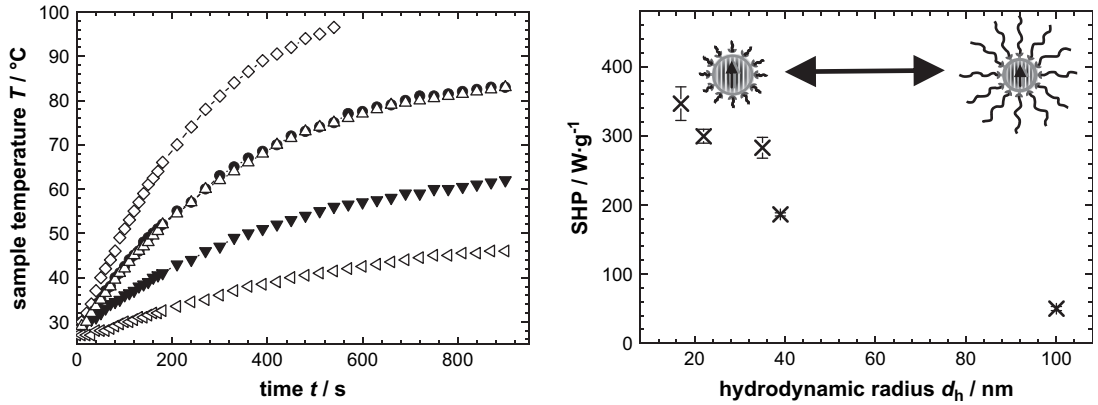

Fig. 7. Magnetic heating results on Co@RA (open upright triangles) and Co@PCL samples (Co@PCL17, filled circles; Co@PCL23, filled downward triangles; Co@PCL27, open rhombs; Co@PCL32, open sideward triangles).

power of the particles from the initial slope of the graph (Fig. 7), with:

$$\mathrm{SHP} = \frac{c_\mathrm{p}}{\mu_{\mathrm{Co,disp}}} \frac{\mathrm{d}T}{\mathrm{d}t} \tag{3}$$

The resulting temperature profiles are shown in Fig. 7 together with obtained SHP values for the different samples. The fluids show a considerable temperature rise within minutes, depending on the cobalt content of the fluids and their respective heating capacities. From the relation of the SHP on characteristic frequencies obtained from AC susceptometry [6], it is found that the faster the particles are able to rotate, the higher the transferred energy into heat. This is in accordance with the above considerations. However, the relationship is not linear, as would be the case if heating power of a single rotation would be constant for the investigated particles. In contrast to this, the SHP/f ratio is increasing with shell thickness. Future experiments will give more insight into the impact of the shell and internal friction on the heat evolution and transfer of such systems.

4. Conclusion

Decorating blocked magnetic Co particles with a poly(ε-caprolactone) shell of adjustable thickness is possible via different pathways, including post-precipitation–functionalization of cobalt particles, and one-pot synthesis of the hydroxy-functional particulate macroinitiators, and subsequent surface-initiated polymerization of ε-caprolactone. We obtain hybrid core–shell particles with high grafting density and adjustable shell thickness, resulting in a brush-like architecture and hydrodynamic diameters in toluene between 21 nm and 55 nm.

Due to the hydrodynamic nature of the magnetization reversal, the effective conversion of magnetic energy to heat energy is shown to be influenced by the shell thickness. In particular, magnetic heating experiments result in decreasing AC loss values for hydrodynamically bigger particles at constant frequency and core size.

The materials may be of interest for microfluidic pump systems or other nanoactuator systems.

Acknowledgement

Funding is obtained from the DFG (Emmy Noether program and SPP 1104) and the Fonds der Chemischen Industrie. Thanks to Prof. Dr. Filipp Oesterhelt, HHU Düsseldorf, for AFM and Prof. Dr. S. Odenbach, TU Dresden, for VSM.

References

[1] Giri S, Trewyn BG. Angew Chem Int Ed 2005;44:5028.
[2] Carpenter EE, Sangregorio C, O'Connor CJ. IEEE Trans Magn 1999;35:3496.
[3] Jun CH, Park YJ. Chem Commun 2006:1619.
[4] Fannin PC. Adv Chem Phys 1998;104:181.
[5] Einstein A. Investigations on the theory of Brownian movement. New York: Dover; 1956.
[6] Feyen M, Heim E, Ludwig F, Schmidt AM, accepted for publication.
[7] Thomas JR. J Appl Phys 1966;37:2914.
[8] Hess PH, Parker Jr PH. J Appl Polym Sci 1966;10:1915.
[9] Platonova OA, Bronstein LM, Solodovnikov SP, Yanovskaya IM, Obolonkova S, Valetsky PM, et al. Colloid Polym Sci 1997;275:426.
[10] Rutnakornpituk M, Thompson MS, Harris LA, Farmer KE, Esker AR, Riffle JS, et al. Polymer 2002;43:2337.
[11] Diana FS, Lee SH, Petroff PM, Kramer EJ. Nano Lett 2003;3:891.
[12] Liu G, Yan X, Lu Z, Curda SA, Lal J. Chem Mater 2005;17:4895.
[13] Korth BD, Keng P, Shim I, Bowles S, Tang C, Kowalewski T, et al. J Am Chem Soc 2006;128:6562.
[14] Burke NAD, Stoever HDH, Dawson FP. Chem Mater 2002;14:4752.
[15] Butter K, Bomans PHH, Frederik PM, Vroege GJ, Philipse AP. Nat Mater 2003;2:88.
[16] von Werne T, Patten TE. J Am Chem Soc 2001;123:7497.
[17] Vestal CR, Zhang ZJ. J Am Chem Soc 2002;124:14312.
[18] Fukuda T, Takano M. Polymer 2004;45:2231.
[19] Gravano SM, Dumas R, Liu K, Patten T. J Polym Sci Part A Polym Chem 2005;43:3675.
[20] Gelbrich T, Feyen M, Schmidt A. Macromolecules 2006;39:3469.
[21] Lahann J, Langer R. Macromol Rapid Commun 2001;22:968.
[22] Möller M, Nederberg F, Lim LS, Kange R, Hawker CJ, Hedrick JL, et al. J Polym Sci Part A Polym Chem 2001;39:3529.
[23] Choi IS, Langer R. Macromolecules 2001;34:5361.
[24] Husemann M, Mecerreyes D, Hawker CJ, Hedrick LJ, Shah R, Abbott NL. Angew Chem Int Ed 1999;38:647.
[25] Schmidt AM. Macromol Rapid Commun 2005;26:93.
[26] Lattuada M, Hatton TA. Langmuir 2007;23:2158.
[27] Bönnemann H, Brijoux W, Brinkmann R, Matoussevitch N, Waldöfner N, Palina N, et al. Inorg Chim Acta 2003;350:617.
[28] Puntes VF, Krishnan KM, Alivisatos AP. Appl Phys Lett 2001;78:2187.
[29] Frait Z, Ondris M. Czech J Phys 1961;11:463.
[30] Alexander S. J Phys 1977;38:983.
[31] de Gennes PG. Macromolecules 1980;13:1069.
[32] Biver C, Hariharan R. Macromolecules 1997;30:1787.